Exploring chalcone-sulfonyl piperazine hybrids as anti-diabetes candidates: Design, synthesis, biological evaluation, and molecular docking study

Narges Hosseini Nasab
Kongju National University
Hussain Raza
Kongju National University
Young Seok Eom
Kongju National University
Fahad Hassan Shah
Kongju National University
Song Ja Kim (ksj85@kongju.ac.kr)
Kongju National University

Research Article

Keywords: Sulfonyl-piperazinyl-chalcone, alpha-glucosidase inhibitor, alpha-amylase inhibitor, cytotoxicity, kinetic mechanism, molecular docking

Posted Date: December 5th, 2023

DOI: https://doi.org/10.21203/rs.3.rs-3696150/v1

Additional Declarations: No competing interests reported.

Exploring chalcone-sulfonyl piperazine hybrids as anti-diabetes candidates: Design, synthesis, biological evaluation, and molecular docking study

Narges Hosseini Nasab, Hussain Raza, Young Seok Eom, Fahad Hassan Shah, Song Ja Kim*

Department of Biological Sciences, Kongju National University, Gongju, 32588, Republic of Korea

*Corresponding author: Prof. Song Ja Kim, Department of Biological Sciences, College of Natural Sciences, Kongju National University, Gongju 32588, Republic of Korea. E-mail: ksj85@kongju.ac.kr

Narges Hosseini Nasab, ORCID: 0000-0002-4916-6023

Hussain Raza, ORCID: 0000-0002-3078-6660

Song Ja Kim, ORCID: 0000-0001-6380-256X

Abstract

To combat the rising rates of diabetes mellitus over the world, novel compounds are required. The demand for more affordable and efficient methods of managing diabetes is increasing due to the unavoidable side effects associated with the existing antidiabetic medications. In order to develop inhibitors against alpha-glucosidase and alpha-amylase, various chalcone-sulfonyl piperazine hybrid compounds (**5a**–**k**) were designed and synthesized in this present research. In addition, several spectroscopic methods, including FT-IR, ^{1}H-NMR, ^{13}C-NMR, and HRMS, were used to confirm the exact structures of the synthesized derivatives. All synthetic compounds were evaluated for their ability to inhibit alpha-glucosidase and alpha-amylase *in vitro* using acarbose as the reference standard and they showed excellent to good inhibitory potentials. Compound **5k** exhibited excellent inhibitory activity against alpha-glucosidase (IC_{50} = 0.31 ± 0.01 μM) and alpha-amylase (IC_{50} = 4.51 ± 1.15 μM), which is 27-fold more active against alpha-glucosidase and 7-fold more active against alpha-amylase compared to acarbose, which had IC_{50} values of 8.62 ± 1.66 μM for alpha-glucosidase and 30.97 ± 2.91 μM for alpha-amylase. It was discovered from the Lineweaver-Burk plot that **5k** exhibited competitive inhibition against alpha-glucosidase. Furthermore, cytotoxicity screening assay results against human fibroblast HT1080 cells showed that all compounds had a good level of safety profile. To explore the binding interactions of the most active compound (**5k**) with the active site of enzymes, molecular docking research was also conducted, and the results obtained supported the experimental data.

Keywords: Sulfonyl-piperazinyl-chalcone, alpha-glucosidase inhibitor, alpha-amylase inhibitor, cytotoxicity, kinetic mechanism, molecular docking

Introduction

Diabetes mellitus (DM) is a major global health issue characterized by abnormalities in insulin action (type 2 diabetes), insulin secretion (type 1 diabetes), or both, resulting in a range of metabolic disorders, such as hypertension and coronary heart disease, which pose a significant risk to individuals' overall health[1–3]. According to the World Health Organization (WHO) reports, the prevalence of diabetes has surpassed 420 million individuals, and it is projected to increase to over 642 million by the year 2040[4]. The prevailing type, which accounts for approximately 80–90% of all diabetic cases, is type-2 diabetes, leading to high blood glucose levels (hyperglycemia)[5], insulin resistance, and the inadequate production of insulin[6]. Reducing blood glucose levels is a highly effective approach to manage diabetes and prevent its associated complications, such as eye, kidney, heart, and vascular diseases[7].

Disaccharides or polysaccharides of carbohydrates are broken down by various intestinal enzymes, such as alpha-glucosidase and alpha-amylase[8]. Alpha-amylase hydrolyzes dietary starch to maltose and dextrin, which are then transformed into glucose by alpha-glucosidase, leading to an increase in blood glucose levels[9]. Therefore, inhibition of both enzymes is a useful strategy for lowering postprandial hyperglycemia[10]. In fact, these two enzymes may be the primary targets for the development of lead medications for the treatment of diabetes.

Acarbose, voglibose, and miglitol are some examples of alpha-glucosidase inhibitors that effectively delay the absorption of sugars from the gut and are used therapeutically to treat diabetes. However, their less frequent utilization can be attributed to their relatively high cost and significant side effects, such as stomachache, diarrhea, and flatulence[11, 12]. Therefore, creating novel small hybrid molecules that act as inhibitors of both alpha-amylase and alpha-glucosidase is a crucial emphasis in medicinal chemistry.

Chalcones are open chain flavonoids and predominantly biosynthesized by plants, but they can also be obtained through numerous synthetic methodologies. Chalcone consists of two aromatic rings that are connected by a three-carbon system, known as an alpha, beta unsaturated carbonyl system[13]. Their simple chemistry, ease of synthesis, and diversity of substituents make them a subject of great fascination among researchers in the 21st Century. They also display a wide range of therapeutic activities, including anti-inflammatory[14], anticancer[15], antioxidants[16], antihypertensive[17], antiviral[18], and antimicrobial[19]. Additionally, chalcones have been identified as potent antidiabetic agents[20, 21]. Fig. 1 displays some chalcone compounds (A–D) exhibiting alpha-amylase and alpha-glucosidase inhibitory activity[22, 23].

Heterocycles are an important class with biological and pharmacological significance that contain at least one ring and an element other than carbon[24]. Heterocycles incorporating nitrogen are extremely important and are the focus of a lot of research[25]. Among these, piperazine, which is a significant six-membered cyclic molecule containing two nitrogen atoms in positions 1 and 4, holds particular importance in the field of medicinal chemistry. This moiety is present in numerous well-known medications with a wide range of therapeutic applications, including antipsychotics[26, 27], antihistamines[28, 29], antianginals[30, 31], antidepressants[32, 33], cancer treatments[34, 35], antivirals[36, 37], and cardio protectors[38, 39]. It is also important to note that the oral DPP-4 inhibitor Teneligliptin, which contains piperazine, has been licensed for the treatment of type-II diabetes[40] (Fig. 1).

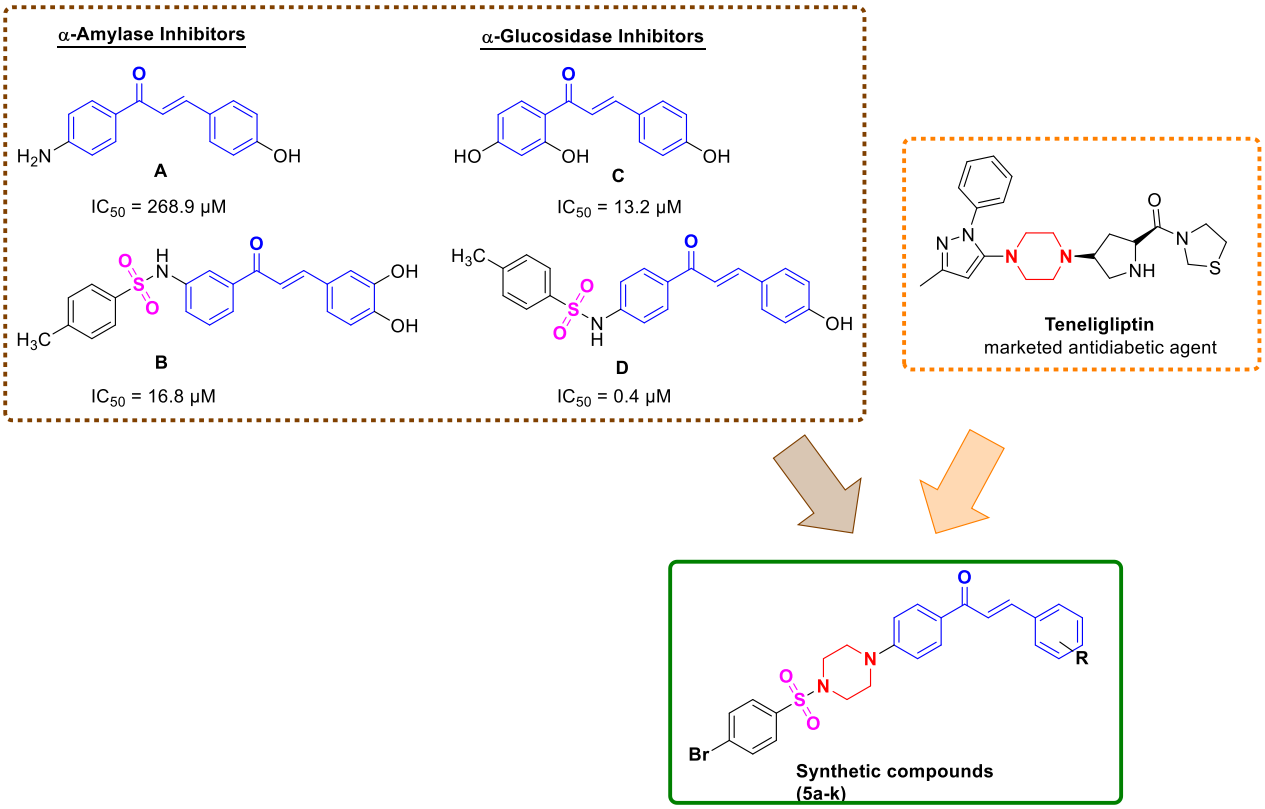

Fig. 1. Design strategy of novel chalcone-sulfonyl piperazine derivatives as new antidiabetic agents based on molecular hybridization of pharmacophoric units of potent chalcone reported alpha-glucosidase and alpha-amylase inhibitors A–D and marketed antidiabetic agent.

To enhance the design and synthesis of hybrid analogs with improved biological potency, molecular hybridization is an invaluable and potent tool[41]. The main goal of this method is to integrate two or more different pharmacophore moieties into a single molecule with a common scaffold, which may have more advantages over standard drugs. Our research team is persistently engaged in the design and synthesis of diverse heterocyclic scaffolds to explore potent therapeutic and inhibitors options[42–46]. Therefore, in our present research, we are combining the three biologically significant moieties of chalcone, sulfonyl, and piperazine utilizing molecular hybridization to create new hybrid compounds that are effective alpha-amylase and alpha-glucosidase inhibitors. Moreover, we conducted kinetic mechanism studies and evaluated cytotoxicity activity, and the outcomes of all these investigations are correlated with the results obtained from molecular docking studies.

Results and discussion

Chemistry

Scheme 1 illustrates the synthetic processes used to produce the target compounds **5a**–**k**. Initially, 4′-piperazinoacetophenone (**1**) and 4-bromobenzenesulfonyl chloride (**2**) were reacted in pyridine at room temperature under a nitrogen atmosphere for 24 hours to produce 4-bromophenylsulfonyl-piperazinyl-acetophenone (**3**) in excellent yield (90%). The target compounds (**5a**–**k**) were synthesized in reasonable yield

(40%–81%) by subjecting compound **3** to Claisen-Schmidt condensation with various aldehydes (**4a**–**k**) in the presence of NaOH in EtOH under reflux conditions.

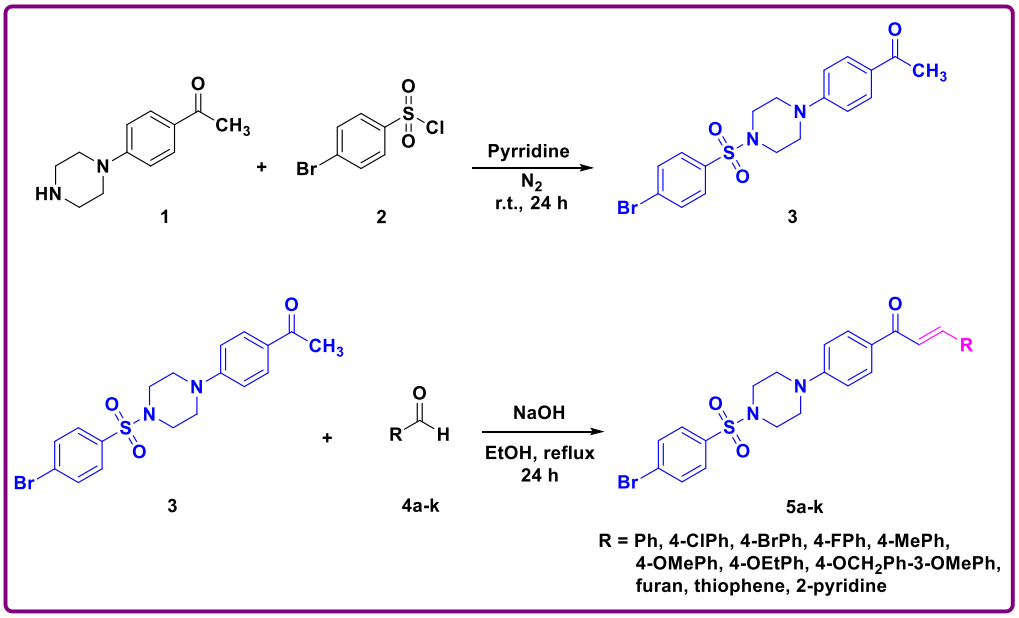

Scheme 1. Synthetic routes of 1-(4-{4-[(4-bromophenyl)sulfonyl]piperazin-1-yl}phenyl)-3-phenyl-prop-2-en-1-one (**5a**–**k**) derivatives.

Biology

Alpha-glucosidase and alpha-amylase inhibitory activity and structure-activity relationship (SAR)

All the compounds (**5a**–**k**) were subjected to *in vitro* assessment to evaluate their inhibitory potential against alpha-glucosidase and alpha-amylase enzymes. The results demonstrated that these molecules displayed excellent to good inhibitory activity, as evidenced by their IC_{50} values (**Table 1**). Among these series, compound **5k** exhibited a significant inhibitory potential, as indicated by its IC_{50} value of 0.31 ± 0.01 µM against alpha-glucosidase and 4.51 ± 1.15 µM against alpha-amylase. Notably, these values were superior to those of the standard reference acarbose, which displayed IC_{50} values of 8.62 ± 1.66 µM and 30.97 ± 2.91 µM against alpha-glucosidase and alpha-amylase, respectively.

Structure-activity relationship (SAR) studies were conducted to examine the impact of different moieties (R) on the activities of alpha-glucosidase and alpha-amylase. Compound **5a**, which contains an unsubstituted phenyl ring, exhibited an IC_{50} value of 14.66 ± 0.81 µM for alpha-glucosidase and an IC_{50} value of 26.06 ± 2.81 µM for alpha-amylase. Comparatively, it demonstrated better activity than acarbose (IC_{50} = 30.97 ± 2.91 µM) in inhibiting alpha-amylase. However, it did not demonstrate superior activity compared to acarbose (IC_{50} = 8.62 ± 1.66 µM) in inhibiting alpha-glucosidase. This suggests that the phenyl group may have a stronger affinity for the active site of alpha-amylase when compared to acarbose. Compound **5a**, was also explored for its anti-inflammatory

properties (with swelling degree of 3.7 ± 0.9 mg) by Li et al[47]. However, it did not exhibit significant activity when compared to celecoxib (swelling degree = 1.6 ± 0.7 mg).

Compounds **5b**–**5d**, which possess electron-withdrawing groups at the *para* position of the phenyl ring, exhibited better inhibition activity against both alpha-glucosidase and alpha-amylase compared to **5a** (unsubstituted phenyl ring) and even outperform the standard acarbose. Among these compounds, **5d** (IC_{50} = 0.63 ± 0.01 µM) with a fluoro group demonstrated better activity against alpha-glucosidase compared to **5b** (IC_{50} = 2.61 ± 0.21 µM) with a chloro group and **5c** (IC_{50} = 5.03 ± 0.79 µM) with a bromo group. This improved activity can be attributed to the specific electronic and steric properties of the fluorine substituent. The smaller size of the fluorine substituent enables a better fit within the active site of alpha-glucosidase, enhancing the interactions with the active site residues. Furthermore, fluorine, with its high electronegativity, affects the electron density distribution in the molecule. This electronic effect may further strengthen the interactions between the 4-fluoro compound and the active site residues of alpha-glucosidase, resulting in enhanced inhibitory activity.

Among compounds **5b**–**5d**, compound **5c** (IC_{50} = 5.71 ± 0.53 µM) displayed better activity against alpha-amylase. This can be attributed to the larger size of the bromo group, which allowed for a more optimal fit within the active site of alpha-amylase. The increased size of the bromo substituent potentially facilitates stronger interactions with the active site residues, resulting in enhanced binding and inhibition of the enzyme's activity.

Compounds **5e**–**5g** displayed enhanced inhibitory activity against both alpha-glucosidase and alpha-amylase compared to the standard acarbose, owing to the presence of electron-donating groups at the *para* position of the phenyl ring. Among these compounds, compound **5e** (IC_{50} = 0.36 ± 0.01 µM), which contains a methyl group, exhibited superior activity against alpha-glucosidase compared to compound **5f** (IC_{50} = 2.98 ± 0.19 µM) with a methoxy group and compound **5g** (IC_{50} = 47.84 ± 1.03 µM) with an ethoxy group. It can be attributed to the relatively small size of methyl group, allowing for better fitting and accommodation within the active site of alpha-glucosidase. The weak activity of the ethoxy group in compound **5g** compared to the methyl and the methoxy groups against alpha-glucosidase can be attributed to two main factors. Firstly, the ethoxy group is larger in size, which may lead to steric hindrance and less favorable interactions with the active site residues of alpha-glucosidase. Secondly, the ethoxy group is less electron-donating than the methyl and methoxy groups, leading to a lower distribution of electron density within the molecule. This reduced electron density distribution can weaken the interactions between compound **5g** and the active site residues of alpha-glucosidase. Compound **5f** (IC_{50} = 7.58 ± 0.83 µM), containing the methoxy group, exhibited better activity against alpha-amylase compared to compound **5e** (IC_{50} = 9.66 ± 0.79 µM) with the methyl group and compound **5g** (IC_{50} = 43.11 ± 1.56 µM) with the ethoxy group. This observation can be attributed to the electronic properties of the methoxy group, which is a strong electron-donating group. The electron-donating nature of the methoxy group likely contributes to its improved activity by facilitating stronger interactions with the active site of alpha-amylase.

The moderate activity observed for compound **5h** (IC_{50} = 13.42 ± 1.66 µM for alpha-glucosidase and IC_{50} = 32.60 ± 4.84 µM for alpha-amylase), which combines benzyloxy and methoxy groups on the phenyl ring, against both alpha-glucosidase and alpha-amylase can be attributed to the presence of bulkier substituents. The larger size of

the benzyloxy and methoxy groups introduces steric hindrance, which can influence the optimal fit of the compound within the active sites of both enzymes.

Compound **5i** (IC_{50} = 7.32 ± 0.92 µM for alpha-glucosidase and IC_{50} = 11.13 ± 0.43 µM for alpha-amylase), which contains a thiophene moiety, demonstrated superior activity compared to compound **5j** (IC_{50} = 30.79 ± 6.28 µM for alpha-glucosidase and IC_{50} = 31.75 ± 6.23 µM for alpha-amylase), which contains a furan moiety, against both alpha-glucosidase and alpha-amylase. This can be attributed to two main factors. Firstly, the sulfur atom possesses a higher electronegativity than the oxygen atom and this higher electronegativity of sulfur facilitates stronger interactions between thiophene and the active site residues of the enzymes. Secondly, the greater aromatic character of thiophene can enhance its stability and increase its affinity for the active sites of alpha-glucosidase and alpha-amylase. The antibacterial properties of compound **5i** were evaluated by Li et al[48]. against *Bacillus subtilis*, *Escherichia coli*, and *Staphylococcus aureus Rosenbach*. In comparison to reference standards including Ofloxacin, Levofloxacin, and Moxifloxacin, it displayed a moderate level of activity.

Compound **5k** (IC_{50} = 0.31 ± 0.01 µM for alpha-glucosidase and IC_{50} = 4.51 ± 1.15 µM for alpha-amylase), which possesses a pyridine scaffold, exhibited the most significant activity against both alpha-glucosidase and alpha-amylase compared to other compounds and even standard acarbose. The literature demonstrates that nitrogen atoms often participate in hydrogen bonding interactions at enzyme binding sites, which helps ligands fit properly within the cavity[5]. There were two reasons for pyridine potent activity. First, the pyridine scaffold offered a unique chemical structure with specific functional groups that can effectively interact with the active sites of the enzymes. The nitrogen atom in the pyridine ring possesses a lone pair of electrons, which can participate in hydrogen bonding and other favorable interactions with the active site residues of alpha-glucosidase and alpha-amylase. Secondly, the aromatic nature of the pyridine ring enhanced its stability and affinity for the active sites of alpha-glucosidase and alpha-amylase. The conjugated π-electron system in the pyridine scaffold promoted favorable π-π interactions with aromatic residues in the active sites, further strengthening the binding and inhibitory activity. Compound **5k** exhibited remarkable potential, both *in vitro* and *in silico* analyses, suggesting that this compound could play a pivotal role in affecting the targets. In the context of alpha-glucosidase, it formed a hydrogen bond with LYS480 through its nitrogen unit in the pyridine ring, hydrophobic interactions with VAL451 and established a π-anion interaction with ASP452 via its pyridine ring. On the other hand, in the case of alpha-amylase, it established hydrophobic interaction with TRP59 via piperazine ring. Hydrogen bonds are formed with ARG195 and GLN63 through the sulfonyl and carbonyl units, respectively. Furthermore, a π-anion interaction occurred with ASP300 through the pyridine ring, and a π-π stacked interaction established with HIS299 and TRP59, involving the pyridine and bromophenyl rings.

Table 1. alpha-Glucosidase and alpha-amylase inhibitory activities of synthesized compounds (**5a**–**k**)

Compounds	R	alpha-Glucosidase IC_{50} ± SEM (µM)	alpha-Amylase IC_{50} ± SEM (µM)
5a	Ph	14.66 ± 0.81	26.06 ± 2.81
5b	4-ClPh	2.61 ± 0.21	11.74 ± 1.35
5c	4-BrPh	5.03 ± 0.79	5.71 ± 0.53

5d	4-FPh	0.63 ± 0.01	10.12 ± 0.44
5e	4-MePh	0.36 ± 0.01	9.66 ± 0.79
5f	4-OMePh	2.98 ± 0.19	7.58 ± 0.83
5g	4-OEtPh	47.84 ± 1.03	43.11 ± 1.56
5h	4-OCH_2Ph-3-OMePh	13.42 ± 1.66	32.60 ± 4.84
5i	thiophene	7.32 ± 0.92	11.13 ± 0.43
5j	furan	30.79 ± 6.28	31.75 ± 6.23
5k	**2-pyridine**	**0.31 ± 0.01**	**4.51 ± 1.15**
Acarbose		8.62 ± 1.66	30.97 ± 2.91

SEM= Standard error of the mean; values are expressed in mean ± SEM.

Kinetic analysis

To gain insight into the inhibitory mechanism of the synthesized compounds on alpha-glucosidase, an inhibition kinetics study was conducted. This study aimed to determine the inhibition type and the inhibition constant of the most potent compound **5k**, as identified through our IC_{50} results. During our analysis of the enzyme kinetics, a set of straight lines was observed in the Lineweaver-Burk plot of 1/V (inverse of reaction velocity) versus 1/[S] (inverse of substrate concentration) at various inhibitor concentrations. In the Lineweaver-Burk plot of compound **5k**, it was observed that the slopes of the lines were not significantly affected, indicating that V_{max} (maximum reaction velocity) remained constant. However, with increasing concentration, K_m (Michaelis constant) showed an increase while V_{max} remained relatively unchanged. The observed pattern suggests that compound **5k** acts as a competitive inhibitor of alpha-glucosidase (Fig. 2A). Additionally, Fig. 2B illustrates the relationship between the slope and the concentration of **5k**, enabling the determination of the EI dissociation constant. By analyzing the concentration of **5k** in relation to the slope, a *K*i value of 0.4 µM was calculated.

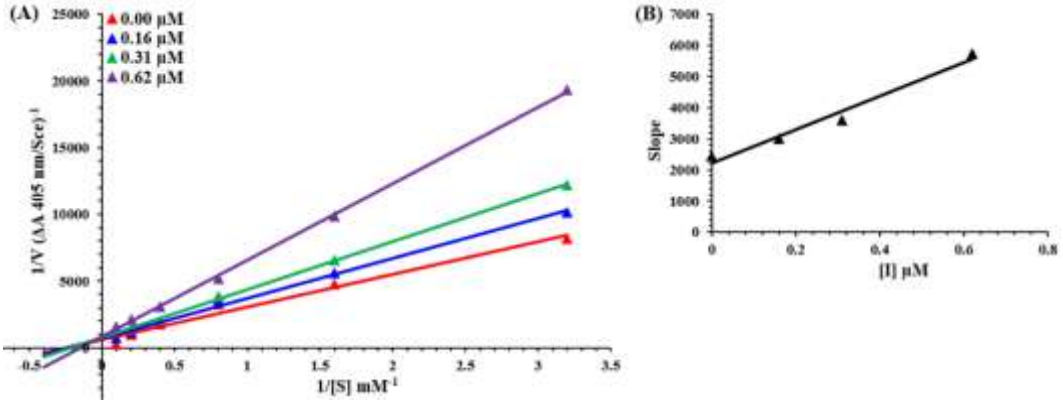

Fig. 2. Lineweaver–Burk plots for inhibition of alpha-glucosidase in the presence of compound **5k**. (**A**) Concentrations of **5k** were 0.00, 0.16, 0.31 and 0.62 mM. (**B**). The insets display the plot of the slope as a function

of inhibitor **5k** concentrations, allowing for the determination of the inhibition constant. The lines on the plot were generated through linear least squares fitting.

Cell viability

The impact of the synthesized compounds (**5a**–**k**) on the viability of human fibroblast HT1080 cells was assessed using an MTT assay. The cells were incubated in 96-well plates until reaching 70% density for 24 hours. Subsequently, the cells were treated with the compounds (**5a**–**k**) as well as acarbose, employed as a positive control for comparative purposes. Concentrations of 10, 20, 30, 40, 50, 60, and 100 μM were utilized for both the synthesized compounds and acarbose. The effects on cell viability were assessed, and the corresponding results are outlined in **Table 2**. Based on these findings, it can be inferred that all our synthesized compounds displayed a relatively safe profile. The control group, which was treated with acarbose, exhibited a cell viability of approximately 79% at the highest concentration of 100 μM. Some compounds demonstrated an improved safety profile in comparison to acarbose, while others (**5a**, **5b**, **5e**, **5f**, and **5i**) exhibited a similar safety profile to that of acarbose. Additionally, compounds **5c** (89%), **5g** (93%), **5h** (85%), **5j** (87%), and **5k** (82%) were identified as the safest, even at the highest concentration (100 μM), when compared to acarbose (79%). Hence, these compounds show great potential as prospective drug candidates in future pharmaceutical development.

Table 2. Cell survived (%) after exposure with compounds for *in vitro* HT1080 fibroblast cell lines.

Compounds	Concentrations (μM, 24 h)						
	10	**20**	**30**	**40**	**50**	**60**	**100**
5a	98	97	95	94	92	90	78
5b	97	95	91	91	89	86	79
5c	98	96	95	95	94	93	89
5d	98	96	–*	–*	–*	–*	–*
5e	99	97	93	89	85	84	74
5f	–*	96	94	90	87	85	72
5g	99	99	98	97	97	96	93
5h	98	98	97	96	91	89	85
5i	–*	96	94	92	90	88	76
5j	–*	–*	–*	–*	–*	97	87
5k	97	95	92	90	88	86	82
acarbose	96	93	91	90	88	84	79

* Indicates no toxicity on the cell viability.

Molecular docking

The refined models of receptors and ligands were used for molecular docking studies. The binding site specified for alpha-glucosidases was MIG, which is attached to these residues (ASP327, ASP443, MET444, ASP542, ASP452), and for alpha-amylase was 3L9 (TYR62, VAL98, HIS101, THR163, LEU168, ASP197, ALA198, LEU162, ARG195, HIS201, TYR151, GLU240, LYS200, ILE235, GLU233, HIS299, and ASP300). Acarbose was used as a standard to compare the docking results with the given ligands. Among these synthesized compounds, compound **5k** showed interaction with both receptors by establishing hydrogen bonds with the specified active site residues, while the other did not establish any notable interactions, which were ignored from further analysis. These results were further analyzed with standard; it was observed that compound **5k** interacted with alpha-glucosidase by forming multiple hydrophobic bonds (Pi-sulfur, Pi-Anion, Pi-Alkyl, and Pi-Pi) and established three hydrogen bonds with LYS480, ARG526, and ARG598 by utilizing the pyridine, sulfonyl, and bromide groups of the compound **5k**. On the other hand, acarbose established multiple hydrogen bonds by exploiting the hydroxyl group in its structure, interacting with ASP203, ASP327, GLU404, ARG526, and ASP542, resulting in a binding energy of 118.1 kJ/mol. In the case of alpha-amylase, the carbonyl and sulfonyl groups of the compound **5k** participated in establishing hydrogen bonds with ARG195 and GLN63, resulting in a binding energy of -101.4 kJ/mol. Here, acarbose formed nine (9) hydrogen bonds and a single hydrophobic interaction with the residues of alpha-amylase, such as TYR151, ARG195, ASP197, LYS200, GLU233, ILE235, ASP300, HIS305, ASP356, and TRP59. These interactions were facilitated by both the hydroxyl and hydrogen groups present in acarbose. By comparing the results of compound **5k** with acarbose, it can be concluded that the activity of **5k** possesses adequate affinity to inhibit the protein activity. This is attributed to the ability of compound **5k** to establish hydrogen bonds with the target residues, which can potentially lead to protein inhibition. The results are illustrated in Figs. 3 and 4.

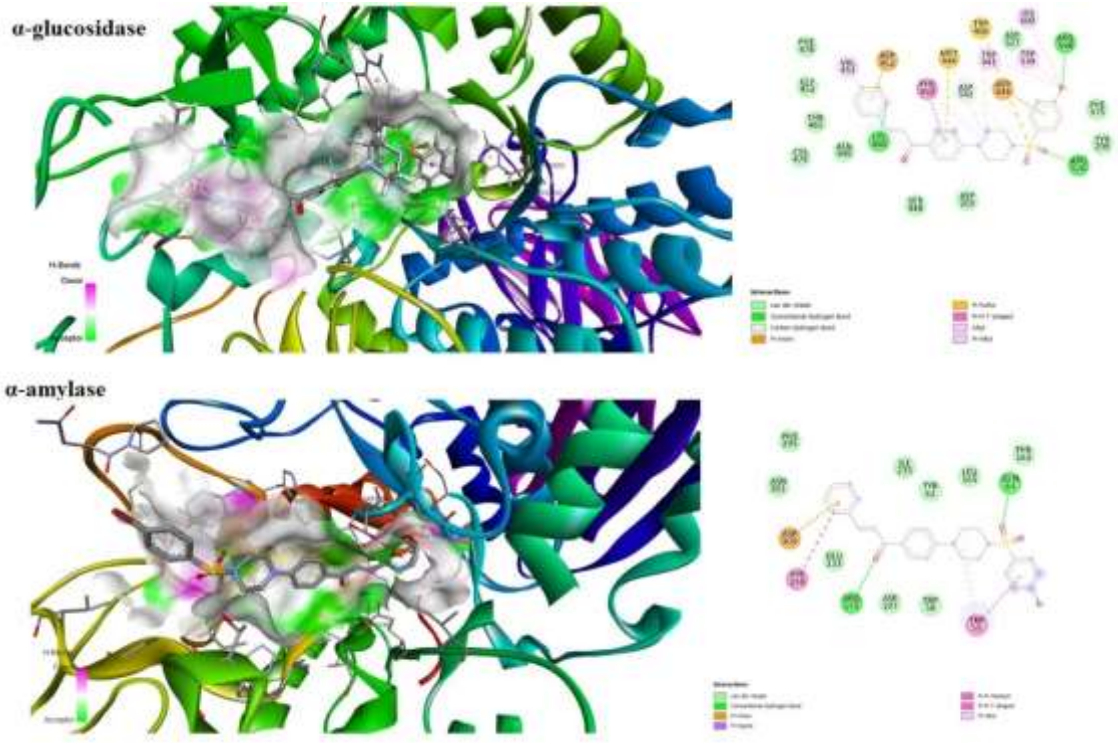

Fig. 3. Docking interaction illustration of **5k** with alpha-glucosidases and alpha-amylase.

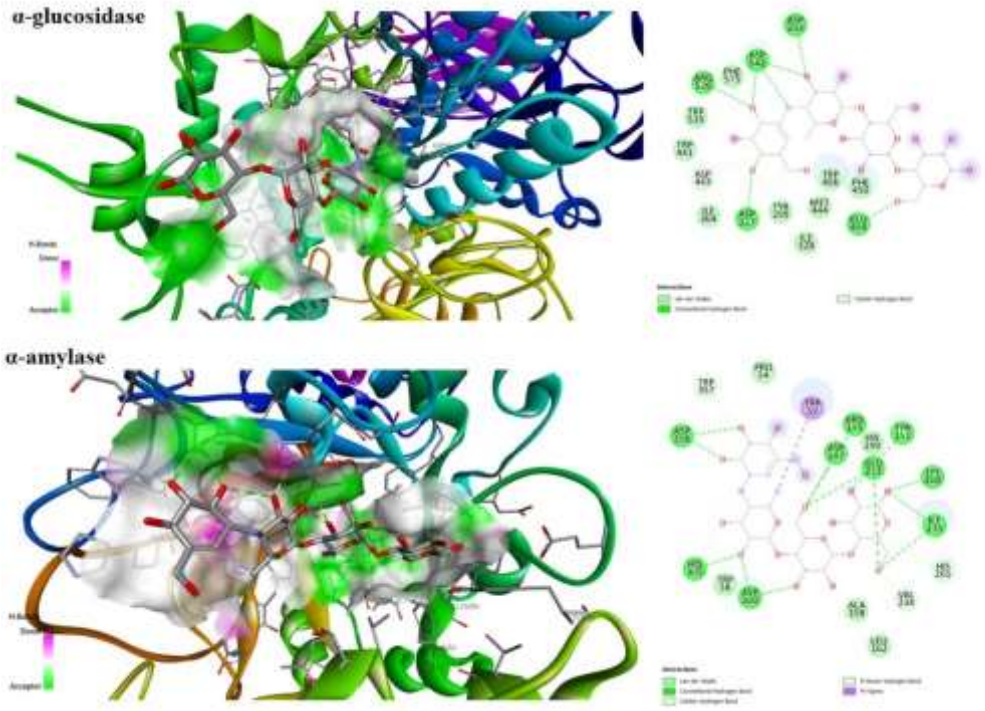

Fig. **4**. Docking interaction illustration of acarbose with alpha-glucosidases and alpha-amylase.

ADMET Prediction Results

The ADMET properties of both the standard drug and compound **5k** were comparatively analyzed (**Table 3**). It was observed that the water solubility value of compound **5k** is -5.58 log mol/L, whereas acarbose has a water solubility value of -1.482 log mol/L. The CaCo-2 permeability and intestinal absorption of compound **5k** were found to be higher than that of acarbose. However, both compounds exhibited similar skin permeability. Additionally, it was observed that acarbose acts as a substrate for P-glycoprotein, whereas compound **5k** inhibits the activity of both P-glycoprotein I and II. The volume of distribution at a steady rate of **5k** was -0.316 log L/kg with no fraction unbound and acarbose was -0.836 log L/kg with a fraction unbound value of 0.505 Fu. Both compounds exhibited minimal BBB and CNS permeability. Acarbose does not affect the activity of CYP variants, whereas compound **5k** acts as a substrate for CYP3A4 and inhibits CYP2C19, CYP2C9, and CYP3A4. The total clearance value for compound **5k** was -0.205 log ml/min/kg, while for acarbose, the value was 0.428. Both compounds are non-toxic; however, they interact with the hERG II protein by inhibiting its function.

Table 3. Chemoinformatic profile of compound **5k** compared with acarbose.

Chemicals	Property	Model Name	Predicted Value	Unit
5k	Absorption	Water solubility	-5.58	Numeric (log mol/L)
	Absorption	Caco-2 permeability	1.153	Numeric (log Papp in 10-6 cm/s)

	Absorption	Intestinal absorption (human)	96.52	Numeric (% Absorbed)
	Absorption	Skin Permeability	-2.756	Numeric (log Kp)
	Absorption	P-glycoprotein substrate	No	Categorical (Yes/No)
	Absorption	P-glycoprotein I inhibitor	Yes	Categorical (Yes/No)
	Absorption	P-glycoprotein II inhibitor	Yes	Categorical (Yes/No)
	Distribution	VDss (human)	-0.316	Numeric (log L/kg)
	Distribution	Fraction unbound (human)	0	Numeric (Fu)
	Distribution	BBB permeability	-0.897	Numeric (log BB)
	Distribution	CNS permeability	-2.119	Numeric (log PS)
	Metabolism	CYP2D6 substrate	No	Categorical (Yes/No)
	Metabolism	CYP3A4 substrate	Yes	Categorical (Yes/No)
	Metabolism	CYP1A2 inhibitor	No	Categorical (Yes/No)
	Metabolism	CYP2C19 inhibitor	Yes	Categorical (Yes/No)
	Metabolism	CYP2C9 inhibitor	Yes	Categorical (Yes/No)
	Metabolism	CYP2D6 inhibitor	No	Categorical (Yes/No)
	Metabolism	CYP3A4 inhibitor	Yes	Categorical (Yes/No)
	Excretion	Total Clearance	-0.205	Numeric (log ml/min/kg)
	Excretion	Renal OCT2 substrate	No	Categorical (Yes/No)
	Toxicity	AMES toxicity	No	Categorical (Yes/No)
	Toxicity	Max. tolerated dose (human)	0.348	Numeric (log mg/kg/day)
	Toxicity	hERG I inhibitor	No	Categorical (Yes/No)
	Toxicity	hERG II inhibitor	Yes	Categorical (Yes/No)
	Toxicity	Oral Rat Acute Toxicity (LD50)	2.779	Numeric (mol/kg)
	Toxicity	Oral Rat Chronic Toxicity (LOAEL)	1.446	Numeric (log mg/kg_bw/day)
	Toxicity	Skin Sensitization	No	Categorical (Yes/No)
	Toxicity	T.Pyriformis toxicity	0.431	Numeric (log ug/L)
	Toxicity	Skin Sensitization	No	Categorical (Yes/No)
Acarbose	Absorption	Water solubility	-1.482	Numeric (log mol/L)
	Absorption	Caco-2 permeability	-0.481	Numeric (log Papp in 10-6 cm/s)
	Absorption	Intestinal absorption (human)	4.172	Numeric (% Absorbed)
	Absorption	Skin Permeability	-2.735	Numeric (log Kp)
	Absorption	P-glycoprotein substrate	Yes	Categorical (Yes/No)
	Absorption	P-glycoprotein I inhibitor	No	Categorical (Yes/No)
	Absorption	P-glycoprotein II inhibitor	No	Categorical (Yes/No)
	Distribution	VDss (human)	-0.836	Numeric (log L/kg)
	Distribution	Fraction unbound (human)	0.505	Numeric (Fu)
	Distribution	BBB permeability	-1.717	Numeric (log BB)
	Distribution	CNS permeability	-6.438	Numeric (log PS)
	Metabolism	CYP2D6 substrate	No	Categorical (Yes/No)
	Metabolism	CYP3A4 substrate	No	Categorical (Yes/No)
	Metabolism	CYP1A2 inhibitor	No	Categorical (Yes/No)
	Metabolism	CYP2C19 inhibitor	No	Categorical (Yes/No)
	Metabolism	CYP2C9 inhibitor	No	Categorical (Yes/No)
	Metabolism	CYP2D6 inhibitor	No	Categorical (Yes/No)
	Metabolism	CYP3A4 inhibitor	No	Categorical (Yes/No)
	Excretion	Total Clearance	0.428	Numeric (log ml/min/kg)
	Excretion	Renal OCT2 substrate	No	Categorical (Yes/No)
	Toxicity	AMES toxicity	No	Categorical (Yes/No)
	Toxicity	Max. tolerated dose (human)	0.435	Numeric (log mg/kg/day)
	Toxicity	hERG I inhibitor	No	Categorical (Yes/No)
	Toxicity	hERG II inhibitor	Yes	Categorical (Yes/No)
	Toxicity	Oral Rat Acute Toxicity (LD50)	2.449	Numeric (mol/kg)
	Toxicity	Oral Rat Chronic Toxicity (LOAEL)	5.319	Numeric (log mg/kg_bw/day)
	Toxicity	Skin Sensitization	No	Categorical (Yes/No)
	Toxicity	T.Pyriformis toxicity	16.823	Numeric (log ug/L)

Conclusion

In conclusion, a multi-step synthesis of chalcone-sulfonyl piperazine derivatives was effectively carried out via molecular hybridization, and all compounds were subjected to *in vitro* inhibitory potentials against alpha-glucosidase and alpha-amylase as compared to standard reference acarbose. The synthesized analogues revealed

excellent to good inhibitory potentials, with IC_{50} values for alpha-glucosidase ranging from 0.31 ± 0.01 to 47.84 ± 1.03 μM and for alpha-amylase from 4.51 ± 1.15 to 43.11 ± 1.56 μM. The MTT assay method was employed to demonstrate the cytotoxicity of all compounds on human fibroblast HT1080 cells. The results clearly indicated that all the synthesized compounds exhibit non-toxicity even at high concentrations. A molecular docking study was conducted to investigate the binding interactions between the most active analogue (**5k**) and the active sites of both enzymes. The results displayed that **5k** forms several essential interactions with the active sites of the enzymes. Considering the comprehensive experimental data, these compounds have the potential to emerge as effective medications for the treatment of type-2 diabetes.

Materials and methods

Chemistry

All commercially available chemicals and solvents were utilized without any additional purification. The melting points were determined in open capillary tubes using an uncorrected MPA 160 apparatus from Fisher Scientific (USA). ^{1}H NMR signals were recorded at 400 MHz and ^{13}C NMR at 100 MHz in DMSO-d_6 employing Bruker Avance III (Germany). FT-IR spectra were obtained using a Frontier IR spectrophotometer from Perkin Elmer, USA. High-resolution mass spectra (HRMS) spectra were acquired on UHPLC/High Resolution Mass Spectrometer, Model: 1290 infinity II/Triple TOF 5600 plus (USA). The progression of the reactions was monitored using thin-layer chromatography (TLC) analysis.

General procedure for the synthesized compounds

Synthesis of 1-(4-{4-[(4-bromophenyl)sulfonyl]piperazin-1-yl}phenyl)-ethan-1-one (3)

To initiate the reaction, 2 mmol of 4′-piperazinoacetophenone (**1**) and 5 ml of pyridine were combined under a N_2 atmosphere at 0 °C for a duration of 5 minutes. Subsequently, 2.6 mmol of 4-bromobenzenesulfonyl chloride (**2**) was slowly added to the mixture. The resulting reaction mixture was stirred at room temperature for 24 hours. Upon completion, the mixture was poured into crushed ice and neutralized by HCl (if no precipitate was formed, HCl was added to acidify the solution). The resulting mixture was stirred for an additional 30 minutes and then. Compound **3** was directly employed in the next step without further purification (**Scheme 1**). Compound **3**, yellow solid, yield = 90 %, **Fig**. **S1**: ^{1}H NMR (DMSO-d_6) δ: 2.45 (s, 3H), 3.03 (t, *J*= 4 Hz, 4H), 3.45 (t, *J*= 4 Hz, 4H), 6.95 (d, *J*= 8 Hz, 2H), 7.71 (d, *J*= 8 Hz, 2H), 7.80 (d, *J*= 8 Hz, 2H), 7.89 (d, *J*= 8 Hz, 2H).

Synthesis of 1-(4-{4-[(4-bromophenyl)sulfonyl]piperazin-1-yl}phenyl)-3-phenylprop-2-en-1-one derivatives (5a–k)

Compounds **5a**–**k** were synthesized using a previously reported method from the literature[45, 49, 50]. To a solution containing 1 mmol of compound **3**, pure EtOH was added, and the mixture was stirred for 5 minutes at

0°C. Subsequently, 1.1 mmol of NaOH was added portion wise, followed by the addition of 1 mmol of various aldehydes (**4a**–**k**). The reaction mixture was then refluxed for a duration of 24 hours. Once the reaction was completed, the mixture was poured into crushed ice and neutralized using HCl. The resulting precipitate was stirred at room temperature for 30 minutes and subsequently filtered. The obtained product was recrystallized from EtOH, resulting in the desired chalcones (**5a**–**k**). The physical and spectral data for compounds **5a**–**k**, are listed below.

1-(4-{4-[(4-Bromophenyl)sulfonyl]piperazin-1-yl}phenyl)-3-phenylprop-2-en-1-one (5a) [47]

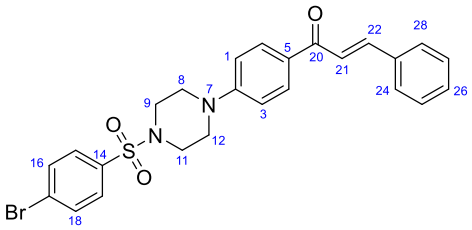

Yellow powder, yield: 81%, m.p: 205–207 ºC. **Fig**. **S2**: IR (KBr) cm^{-1}: 2889, 2854, 1652, 1608, 1588, 1573, 1388, 1350, 1223, 1166, 943. **Fig**. **S3**: [1] HNMR (400 MHz, DMSO-d_6) δ (ppm): 3.05 (t, *J*= 4 Hz, 4H, Pip–CH_2, 9 and 11), 3.49 (t, *J*= 4 Hz, 4H, Pip–CH_2, 8 and 12), 7.01 (d, *J*= 8 Hz, 2H, H–1 and H–3), 7.44-7.48 (m, 3H, H–25, H–26, and H–27), 7.67 (d, *J*= 16 Hz, 1H, H–21), 7.72 (d, *J*= 8 Hz, 2H, H–24 and H–28), 7.86-7.94 (m, 5H, H–4, H–6, H–16, H–18, and H–22), 8.06 (d, *J*= 8 Hz, 2H, H–15 and H–19). **Fig**. **S4**: ^{13}C NMR (100 MHz, DMSO-d_6) δ (ppm): 45.94 (2C, C–9 and C–11), 46.61 (2C, C–8 and C–12), 114.28 (2C, C–1 and C–3), 122.62 (C–21), 127.98 (C–5), 128.23 (C–17), 129.16 (2C, C–24 and C–28), 129.34 (2C, C–25 and C–27), 130.05 (2C, C–15 and C–19), 130.72 (C–26), 131.05 (2C, C–4 and C–6), 133.11 (2C, C–16 and C–18), 134.51 (C–23), 135.44 (C–14), 142.84 (C–22), 153.66 (C–2), 187.05 (C–20).

1-(4-{4-[(4-Bromophenyl)sulfonyl]piperazin-1-yl}phenyl)-3-(4-chlorophenyl)prop-2-en-1-one (5b)

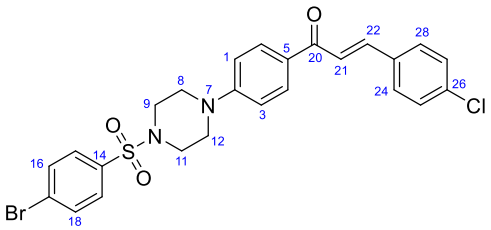

Yellow powder, yield: 48%, m.p: 228–230 ºC. **Fig**. **S5**: IR (KBr) cm^{-1}: 2841, 1649, 1605, 1586, 1387, 1358, 1349, 1221, 1166, 946. **Fig**. **S6**: [1] HNMR (400 MHz, DMSO-d_6) δ (ppm): 3.05 (t, *J*= 4 Hz, 4H, Pip–CH_2, 9 and 11), 3.50 (t, *J*= 4 Hz, 4H, Pip–CH_2, 8 and 12), 7.00 (d, *J*= 12 Hz, 2H, H–1 and H–3), 7.52 (d, *J*= 8 Hz, 2H, H–24 and H–28), 7.66 (d, *J*= 16 Hz, 1H, H–21), 7.71 (d, *J*= 8 Hz, 2H, H–25 and H–27), 7.88-7.97 (m, 5H, H–4, H–6, H–16, H–18, and H–22), 8.06 (d, *J*= 8 Hz, 2H, H–15 and H–19). **Fig**. **S7**: ^{13}C NMR (100 MHz, DMSO-d_6) δ (ppm): 45.94 (2C, C–9 and C–11), 46.58 (2C, C–8 and C– 12), 114.24 (2C, C–1 and C– 3), 123.38 (C–21), 127.99 (C–5), 128.11 (C–17), 129.36 (2C, C–24 and C–28), 130.05 (2C, C–15 and C–19), 130.87 (2C, C–25 and C–27), 131.12 (2C, C–4 and C–6), 133.11 (2C, C–16 and C–18), 134.44 (C–23), 134.49 (C–26), 135.15 (C–14), 141.37 (C–22), 153.70 (C–2), 186.90 (C–20).

1-(4-{4-[(4-Bromophenyl)sulfonyl]piperazin-1-yl}phenyl)-3-(4-bromophenyl)prop-2-en-1-one (5c)

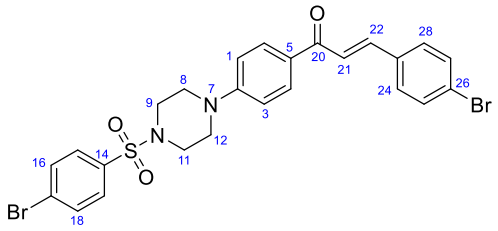

Yellow powder, yield: 76%, m.p: 240–242 ºC. **Fig**. **S8**: IR (KBr) cm^{-1}: 2841, 1648, 1586, 1387, 1349, 1221, 1165, 946. **Fig**. **S9**: [1] HNMR (400 MHz, DMSO-d_6) δ (ppm): 3.05 (t, *J*= 4 Hz, 4H, Pip–CH_2, 9 and 11), 3.50 (t, *J*= 4 Hz, 4H, Pip–CH_2, 8 and 12), 7.00 (d, *J*= 12 Hz, 2H, H–1 and H–3), 7.62-7.67 (m, 3H, H–21, H–24, and H–28), 7.70-7.73 (m, 2H, H–25 and H–27), 7.84 (d, *J*= 8 Hz, 2H, H–4 and H–6), 7.89 (d, *J*= 8 Hz, 2H, H–16 and H–18), 7.96 (d, *J*= 16 Hz, 1H, H–22), 8.06 (d, *J*= 8 Hz, 2H, H–15 and H–19). **Fig**. **S10**: ^{13}C NMR (100 MHz, DMSO-d_6) δ (ppm): 45.94 (2C, C–9 and C–11), 46.58 (2C, C–8 and C–12), 114.24 (2C, C–1 and C–3), 123.45 (C–21), 124.00 (C–26), 127.98 (C–5), 128.09 (C–17), 130.05 (2C, C–15 and C–19), 131.10 (4C, C–4, C–6, C–24, and C–28), 132.29 (2C, C–25 and C–27), 133.11 (2C, C–16 and C–18), 134.50 (C–23), 134.77 (C–14), 141.46 (C–22), 153.71 (C–2), 186.90 (C–20).

1-(4-{4-[(4-Bromophenyl)sulfonyl]piperazin-1-yl}phenyl)-3-(4-fluorophenyl)prop-2-en-1-one (5d)

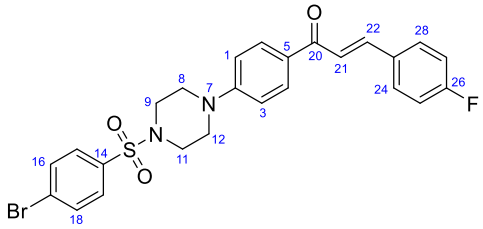

Yellow powder, yield: 46%, m.p: 203–205 ºC. **Fig**. **S11**: IR (KBr) cm^{-1}: 2841, 1649, 1586, 1387, 1349, 1221, 1166, 947. **Fig**. **S12**: [1] HNMR (400 MHz, DMSO-d_6) δ (ppm): 3.05 (t, *J*= 4 Hz, 4H, Pip–CH_2, 9 and 11), 3.49 (t, *J*= 4 Hz, 4H, Pip–CH_2, 8 and 12), 7.01 (d, *J*= 12 Hz, 2H, H–1 and H–3), 7.30 (t, *J*= 8 Hz, 2H, H–25 and H–27), 7.67 (d, *J*= 16 Hz, 1H, H–21), 7.72 (d, *J*= 12 Hz, 2H, H–24 and H–28), 7.87-7.98 (m, 5H, H–4, H–6, H–16, H–18, and H–22), 8.06 (d, *J*= 8 Hz, 2H, H–15 and H–19). **Fig**. **S13**: ^{13}C NMR (100 MHz, DMSO-d_6) δ (ppm): 45.94 (2C, C–9 and C–11), 46.60 (2C, C–8 and C–12), 114.26 (2C, C–1 and C–3), 116.33 (d, *J*= 22 Hz, 2C, C–25 and C–27), 122.50 (C–21), 127.98 (C–5), 128.21 (C–17), 130.04 (2C, C–15 and C–19), 131.06 (2C, C–4 and C–6), 131.47 (d, *J*= 8 Hz, 2C, C–24 and C–28), 132.13 (d, *J*= 3 Hz, C–23), 133.10 (2C, C–16 and C–18), 134.49 (C–14), 141.61 (C–22), 153.66 (C–2), 163.67 (d, *J*= 246 Hz, C–26), 186.96 (C–20). **Fig**. **S14**: HRMS (m/z): [M+H, ^{81}Br] calculated for $C_{25}H_{22}BrFN_2O_3S$, 531.0566; found 531.0566.

1-(4-{4-[(4-Bromophenyl)sulfonyl]piperazin-1-yl}phenyl)-3-(*p*-tolyl)prop-2-en-1-one (5e)

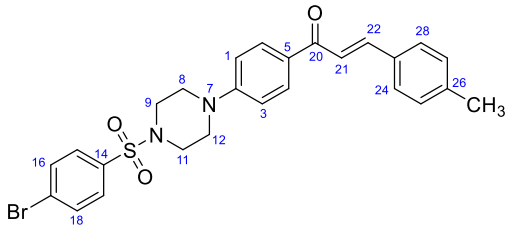

Yellow powder, yield: 71%, m.p: 206–208 °C. **Fig**. **S15**: IR (KBr) cm^{-1}: 2967, 1651, 1591, 1388, 1355, 1222, 1165, 948. **Fig**. **S16**: ^{1} HNMR (400 MHz, DMSO-d_6) δ (ppm): 2.36 (s, 3H, CH_3), 3.05 (t, *J*= 4 Hz, 4H, Pip–CH_2, 9 and 11), 3.49 (t, *J*= 4 Hz, 4H, Pip–CH_2, 8 and 12), 7.00 (d, *J*= 8 Hz, 2H, H–1 and H–3), 7.27 (d, *J*= 8 Hz, 2H, H–25 and H–27), 7.64 (d, *J*= 16 Hz, 1H, H–21), 7.72 (d, *J*= 8 Hz, 2H, H–24 and H–28), 7.76 (d, *J*= 8 Hz, 2H, H–4 and H–6), 7.84-7.90 (m, 3H, H–16, H–18, and H–22), 8.05 (d, *J*= 8 Hz, 2H, H–15 and H–19). **Fig**. **S17**: ^{13}C NMR (100 MHz, DMSO-d_6) δ (ppm): 21.55 (CH_3), 45.95 (2C, C–9 and C–11), 46.63 (2C, C–8 and C–12), 114.29 (2C, C–1 and C–3), 121.54 (C–21), 127.98 (C–5), 128.36 (C–17), 129.18 (2C, C–24 and C–28), 129.97 (2C, C–25 and C–27), 130.05 (2C, C–15 and C–19), 130.98 (2C, C–4 and C–6), 132.71 (C–23), 133.10 (2C, C–16 and C–18), 134.50 (C–14), 140.70 (C–26), 142.91 (C–22), 153.61 (C–2), 187.06 (C–20). **Fig**. **S18**: HRMS (m/z): [M+H, ^{81}Br] calculated for $C_{26}H_{25}BrN_2O_3S$, 527.0827; found 527.0827.

1-(4-{4-[(4-Bromophenyl)sulfonyl]piperazin-1-yl}phenyl)-3-(4-methoxyphenyl)prop-2-en-1-one (5f)

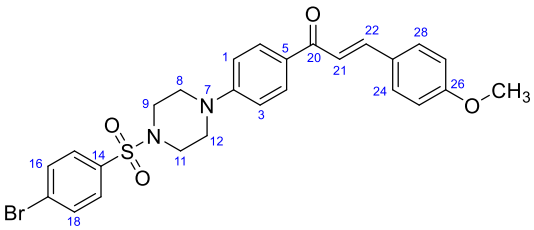

Yellow powder, yield: 44%, m.p: 190–192 °C. **Fig**. **S19**: IR (KBr) cm^{-1}: 2967, 1648, 1598, 1573, 1509, 1387, 1348, 1221, 1165, 947. **Fig**. **S20**: ^{1} HNMR (400 MHz, DMSO-d_6) δ (ppm): 3.05 (t, *J*= 4 Hz, 4H, Pip–CH_2, 9 and 11), 3.48 (t, *J*= 4 Hz, 4H, Pip–CH_2, 8 and 12), 3.83 (s, 3H, OCH_3), 7.01 (dd, *J*= 10, 8 Hz, 4H, H–1, H–3, H–25, and H–27), 7.64 (d, *J*= 16 Hz, 1H, H–21), 7.71 (d, *J*= 12 Hz, 2H, H–24 and H–28), 7.78 (d, *J*= 16 Hz, 1H, H–22), 7.83 (d, *J*= 8 Hz, 2H, H–4 and H–6), 7.89 (d, *J*= 8 Hz, 2H, H–16 and H–18), 8.04 (d, *J*= 8 Hz, 2H, H–15 and H–19). **Fig**. **S21**: ^{13}C NMR (100 MHz, DMSO-d_6) δ (ppm): 45.95 (2C, C–9 and C–11), 46.65 (2C, C–8 and C–12), 55.82 (OCH_3), 114.31 (2C, C–1 and C–3), 114.82 (2C, C–25 and C–27), 120.07 (C–21), 127.99 (C–5), 128.06 (C–17), 128.53 (C–23), 130.05 (2C, C–15 and C–19), 130.89 (2C, C–24 and C–28), 131.00 (2C, C–4 and C–6), 133.10 (2C, C–16 and C–18), 134.45 (C–14), 142.83 (C–22), 153.53 (C–2), 161.53 (C–26), 187.00 (C–20). **Fig**. **S22**: HRMS (m/z): [M+H, ^{81}Br] calculated for $C_{26}H_{25}BrN_2O_4S$, 543.0766; found 543.0766.

1-(4-{4-[(4-Bromophenyl)sulfonyl]piperazin-1-yl}phenyl)-3-(4-ethoxyphenyl)prop-2-en-1-one (5g)

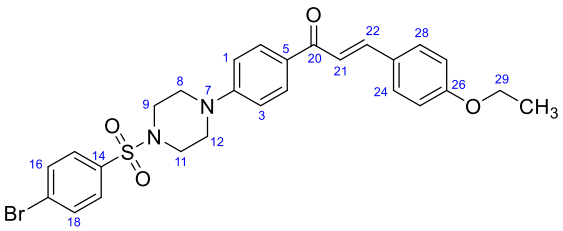

Orange powder, yield: 40%, m.p: 184–186 °C. **Fig**. **S23**: IR (KBr) cm^{-1}: 2967, 1645, 1596, 1569, 1509, 1384, 1361, 1218, 1170, 947. **Fig**. **S24**: ^{1} HNMR (400 MHz, DMSO-d_6) δ (ppm): 1.35 (t, *J*= 8 Hz, 3H, OCH_3), 3.05 (t, *J*= 4 Hz, 4H, Pip–CH_2, 9 and 11), 3.48 (t, *J*= 4 Hz, 4H, Pip–CH_2, 8 and 12), 4.10 (q, *J*= 8 Hz, 2H, CH_2–29), 7.00 (d, *J*= 8 Hz, 4H, H–1, H–3, H–25, and H–27), 7.64 (d, *J*= 16 Hz, 1H, H–21), 7.72 (d, *J*= 8 Hz, 2H, H–24 and H–28), 7.77 (d, *J*= 16 Hz, 1H, H–22), 7.82 (d, *J*= 12 Hz, 2H, H–4 and H–6), 7.89 (d, *J*= 8 Hz, 2H, H–16 and H–18), 8.04 (d, *J*= 8 Hz, 2H, H–15 and H–19). **Fig**. **S25**: ^{13}C NMR (100 MHz, DMSO-d_6) δ (ppm): 15.04 (CH_3), 45.95 (2C, C–9 and C–11), 46.66 (2C, C–8 and C–12), 63.77 (CH_2–29), 114.31 (2C, C–1 and C–3), 115.20 (2C, C–25 and C–27), 119.98 (C–21), 127.91 (C–5), 127.98 (C–17), 128.54 (C–23), 130.06 (2C, C–15 and C–19), 130.89 (2C, C–24 and C–28), 131.02 (2C, C–4 and C–6), 133.11 (2C, C–16 and C–18), 134.46 (C–14), 142.86 (C–22), 153.53 (C–2), 160.83 (C–26), 187.00 (C–20).

1-(4-{4-[(4-Bromophenyl)sulfonyl]piperazin-1-yl}phenyl)-3-(4-(benzyloxy)-3-methoxyphenyl)prop-2-en-1-one (5h)

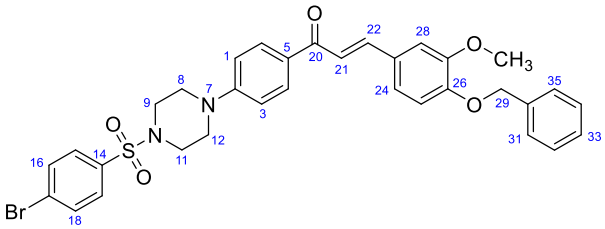

Yellow powder, yield: 54%, m.p: 189–191 ºC. **Fig**. **S26**: IR (KBr) cm^{-1}: 2967, 1645, 1598, 1572, 1506, 1353, 1215, 1162, 951. **Fig**. **S27**: [1] HNMR (400 MHz, DMSO-d_6) δ (ppm): 3.05 (t, *J*= 4 Hz, 4H, Pip–CH_2, 9 and 11), 3.47-3.48 (m, 4H, Pip–CH_2, 8 and 12), 3.88 (s, 3H, OCH_3), 5.16 (s, 2H, CH_2–29), 7.00 (d, *J*= 8 Hz, 2H, H–1 and H–3), 7.11 (d, *J*= 12 Hz, 1H, H–25), 7.34-7.37 (m, 2H, H–24 and H–28), 7.42 (t, *J*= 8 Hz, 2H, H–32 and H–34), 7.47 (d, *J*= 8 Hz, 2H, H–31 and H–35), 7.54 (d, *J*= 1.6 Hz, 1H, H–33), 7.63 (d, *J*= 16 Hz, 1H, H–21), 7.72 (d, *J*= 8 Hz, 2H, H–4 and H–6), 7.80 (d, *J*= 16 Hz, 1H, H–22), 7.89 (d, *J*= 8 Hz, 2H, H–16 and H–18), 8.05 (d, *J*= 8 Hz, 2H, H–15 and H–19). **Fig**. **S28**: ^{13}C NMR (100 MHz, DMSO-d_6) δ (ppm): 45.95 (2C, C–9 and C–11), 46.66 (2C, C–8 and C–12), 56.27 (C–CH_3O), 70.28 (CH_2–29), 111.52 (C–28), 113.57 (C–25), 114.30 (2C, C–1 and C–3), 120.33 (C–21), 123.77 (C–24), 127.99 (C–5), 128.37 (3C, C–17, C–31, and C–35), 128.43 (C–33), 128.56 (C–23), 128.93 (2C, C–32 and C–34), 130.06 (2C, C–15 and C–19), 130.94 (2C, C–4 and C–6), 133.11 (2C, C–16 and C–18), 134.44 (C–14), 137.26 (C–30), 143.28 (C–22), 149.74 (C–27), 150.37 (C–26), 153.55 (C–2), 187.03 (C–20).

1-(4-{4-[(4-Bromophenyl)sulfonyl]piperazin-1-yl}phenyl)-3-(thiophen-2-yl)prop-2-en-1-one (5i) [48]

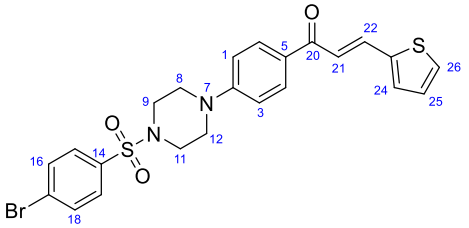

Yellow powder, yield: 65%, m.p: 197–199 ºC. **Fig**. **S29**: IR (KBr) cm^{-1}: 2967, 1651, 1606, 1585, 1385, 1355, 1164, 945. **Fig**. **S30**: [1] HNMR (400 MHz, DMSO-d_6) δ (ppm): 3.05 (t, *J*= 4 Hz, 4H, Pip–CH_2, 9 and 11), 3.48 (t, *J*= 4 Hz, 4H, Pip–CH_2, 8 and 12), 7.00 (d, *J*= 8 Hz, 2H, H–1 and H–3), 7.19 (dd, *J*= 4.9, 3.6 Hz, 1H, H–25), 7.54 (d, *J*= 16 Hz, 1H, H–21), 7.65 (d, *J*= 4 Hz, 1H, H–24), 7.70-7.73 (m, 2H, H–4 and H–6), 7.76 (d, *J*= 4 Hz, 1H, H–26), 7.83 (d, *J*= 16 Hz, 1H, H–22), 7.89 (d, *J*= 8 Hz, 2H, H–16 and H–18), 7.98 (d, *J*= 8 Hz, 2H, H–15 and H–19). **Fig**. **S31**: ^{13}C NMR (100 MHz, DMSO-d_6) δ (ppm): 45.93 (2C, C–9 and C–11), 46.59 (2C, C–8 and C–12), 114.30 (2C, C–1 and C–3), 120.95 (C–21), 127.99 (C–5), 128.08 (C–17), 129.11 (C–25), 130.06 (2C, C–15 and C–19), 130.27 (C–24), 130.88 (2C, C–4 and C–6), 132.65 (C–26), 133.11 (2C, C–16 and C–18), 134.44 (C–14), 135.62 (C–22), 140.47 (C–23), 153.62 (C–2), 186.49 (C–20).

1-(4-{4-[(4-Bromophenyl)sulfonyl]piperazin-1-yl}phenyl)-3-(furan-2-yl)prop-2-en-1-one (5j)

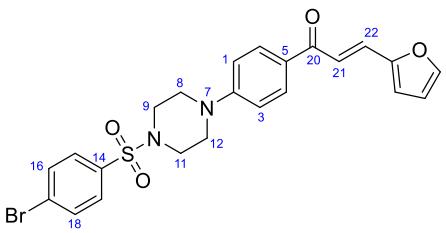

Yellow powder, yield: 63%, m.p: 185–187 °C. **Fig**. **S32**: IR (KBr) cm^{-1}: 2967, 1651, 1599, 1386, 1351, 1229, 1164, 945. **Fig**. **S33**: ^{1} HNMR (400 MHz, DMSO-d_6) δ (ppm): 3.05 (t, *J*= 4 Hz, 4H, Pip–CH_2, 9 and 11), 3.48 (t, *J*= 4 Hz, 4H, Pip–CH_2, 8 and 12), 6.68 (dd, *J*= 3.3, 1.8 Hz, 1H, H–25), 7.00 (d, *J*= 8 Hz, 2H, H–1 and H–3), 7.06 (d, *J*= 4 Hz, 1H, H–24), 7.47-7.56 (m, 2H, H–21 and H–26), 7.70-7.73 (m, 2H, H–4 and H–6), 7.88-7.90 (m, 3H, H–22, H–16, and H–18), 7.96 (d, *J*= 8 Hz, 2H, H–15 and H–19). **Fig**. **S34**: ^{13}C NMR (100 MHz, DMSO-d_6) δ (ppm): 45.93 (2C, C–9 and C–11), 46.58 (2C, C–8 and C–12), 113.46 (C–25), 114.33 (2C, C–1 and C–3), 116.62 (C–24), 119.32 (C–21), 127.99 (C–5), 128.10 (C–17), 129.55 (C–22), 130.05 (2C, C–15 and C–19), 130.80 (2C, C–4 and C–6), 133.11 (2C, C–16 and C–18), 134.45 (C–14), 146.24 (C–26), 151.83 (C–23), 153.61 (C–2), 186.43 (C–20). **Fig**. **S35**: HRMS (m/z): [M+H, ^{81}Br] calculated for $C_{23}H_{21}BrN_2O_4S$, 503.0463; found 503.0462.

1-(4-{4-[(4-Bromophenyl)sulfonyl]piperazin-1-yl}phenyl)-3-(pyridin-2-yl)prop-2-en-1-one (5k)

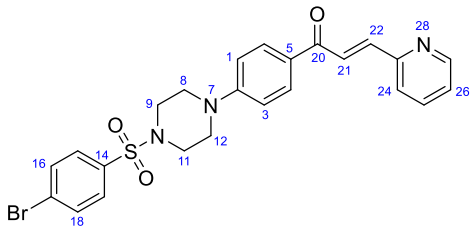

Yellow powder, yield: 60%, m.p: 210–212 °C. **Fig**. **S36**: IR (KBr) cm^{-1}: 2967, 1651, 1599, 1583, 1386, 1351, 1164, 945. **Fig**. **S37**: ^{1} HNMR (400 MHz, DMSO-d_6) δ (ppm): 3.05 (t, *J*= 4 Hz, 4H, Pip–CH_2, 9 and 11), 3.50 (t, *J*= 4 Hz, 4H, Pip–CH_2, 8 and 12), 7.02 (d, *J*= 8 Hz, 2H, H–1 and H–3), 7.41-7.45 (m, 1H, H–26), 7.66 (d, *J*= 12 Hz, 1H, H–21), 7.72 (d, *J*= 8 Hz, 2H, H–4 and H–6), 7.88-7.90 (m, 4H, H–16, H–18, H–24, and H–25), 8.00 (d, *J*= 8 Hz, 2H, H–15 and H–19), 8.13 (d, *J*= 12 Hz, 1H, H–22), 8.68 (d, *J*= 4 Hz, 1H, H–27). **Fig**. **S38**: ^{13}C NMR (100 MHz, DMSO-d_6) δ (ppm): 45.93 (2C, C–9 and C–11), 46.52 (2C, C–8 and C–12), 114.30 (2C, C–1 and C–3), 125.03 (C–26), 125.15 (C–24), 125.67 (C–21), 127.89 (C–5), 127.99 (C–17), 130.05 (2C, C–15 and C–19), 131.07 (2C, C–4 and C–6), 133.11 (2C, C–16 and C–18), 134.48 (C–14), 137.64 (C–25), 142.01 (C–22), 150.44 (C–27), 153.57 (C–23), 153.77 (C–2), 187.08 (C–20). **Fig**. **S39**: HRMS (m/z): [M+H, ^{81}Br] calculated for $C_{24}H_{22}BrN_3O_3S$, 514.0613; found 514.0617.

Biology methodology

Alpha-glucosidase inhibition assay

The inhibitory activities of the synthesized compounds against α-glucosidase were evaluated using a methodology described in the literature [11]. Acarbose was employed as a standard reference drug.

Alpha-amylase inhibition assay

The α-amylase inhibitory activity of the synthesized compounds was assessed using a method described in a previously published study [11].

Alpha-glucosidase kinetic mechanism

Among the inhibitors tested, compound **5k** demonstrated the highest potency (IC_{50} value). Consequently, compound **5k** was selected for kinetic analysis. Several experiments were conducted to calculate the inhibition kinetics of compound **5k** [51]. Various concentrations of **5k** (0.00, 0.16, 0.31, and 0.62) were tested. The

concentration of the substrate, *p*-nitrophenyl-*α*-D-glucopyranoside, ranged from 0.3125 to 10 mM in all the kinetics experiments. The pre-incubation and measurement periods matched those specified in the procedure for the α-glucosidase inhibition assay. The maximal initial velocity was determined from the initial linear portion of absorbance in the first five minutes following the addition of the enzyme at 30 s intervals. To determine the type of enzyme inhibition, Lineweaver-Burk plots were constructed by plotting the inverse of the velocities (1/V) against the inverse of the substrate concentration (1/[S]) in units of mM^{-1}. The dissociation constant (*Ki*) for the enzyme-inhibitor (EI) complex was determined by generating a secondary plot of 1/V versus the inhibitor concentration.

Cell culture and treatment

Human fibroblast HT1080 cells were procured from the Korean Cell Line Bank in Seoul, Korea, and utilized for evaluating the cytotoxicity of the synthesized compounds (**5a**–**k**). The cultivation and treatment procedures were performed according to the methods described in the literature [52].

Cell viability

To determine the cell viability of the compounds, we employed the 3-(4,5-dimethylthiazol-2-yl)-2,5-diphenyltetrazolium bromide (MTT) assay. HT1080 cells were seeded onto 96-well plates at a density of 0.4×10^5 cells/well with three replicate wells per group and incubated in media for 24 hours. The compounds (**5a**–**k**) were treated at different concentrations (10, 20, 30, 40, 50, 60, and 100 µM), while acarbose was employed as a control group at the same concentrations. After 24 hours of incubation, the media was discarded, and 100 µl of 0.5 mg/ml MTT solution, diluted in DMEM, was added to each well for 4 hours. The resulting formazan crystals were solubilized by adding 100 µl of DMSO, and the absorbance of the 96-well plate was measured at 570 nm using a microplate reader (Thermo Fisher, MA, USA).

***In-silico* methodology**

Chemical Structure Preparation

The structures of the synthesized compounds (**5a**–**k**) were prepared for molecular docking studies by converting the Chemdraw format files into mol2 files using Discovery Studio [53] and OpenBabel [54]. The structure of acarbose was retrieved from PubChem and converted to mol2 format using Discovery studio. These structures were hydrogenated polarly and minimized using the PRODRG server [55].

Receptor Structure Preparation

The structures of α-glucosidase and α-amylase were obtained from the Protein Data Bank database, with IDs 3L4W and 4W93, respectively. These structures were prepared by removing water ions and in-bound ligands. Subsequently, they were submitted to the Modrefiner database [56] for structural minimization.

Molecular Docking Studies

The minimized ligands and receptors were uploaded to the iGEMDOCK [57] interface, where the binding site of the ligand was specified to conduct site-directed interactions with the active site residues of the receptors. The selected algorithm for this interaction with the receptors was Standard docking.

ADMET and Physicochemical Properties Prediction

The prediction of ADMET and physiochemical properties for these ligands was conducted using the pKCSM [58] database and SwissADME [59]. The structure of each ligand was converted into canonical SMILES format using OpenBabel and subsequently submitted to the database for ADMET prediction.

Conflict of Interest

The authors have no conflicts of interest to declare that are relevant to the content of this article.

Acknowledgement

This work was supported by the National Research Foundation of Korea (NRF) funded by the

Korean Government (MEST) (2020R1I1A306969914).

References

1. Wang K, Bao L, Ma K, et al (2017) A novel class of α-glucosidase and HMG-CoA reductase inhibitors from Ganoderma leucocontextum and the anti-diabetic properties of ganomycin I in KK-Ay mice. Eur J Med Chem 127:1035–1046
2. Pogaku V, Gangarapu K, Basavoju S, et al (2019) Design, synthesis, molecular modelling, ADME prediction and anti-hyperglycemic evaluation of new pyrazole-triazolopyrimidine hybrids as potent α-glucosidase inhibitors. Bioorg Chem 93:103307
3. Ezati M, Ghavamipour F, Adibi H, et al (2023) Design, synthesis, spectroscopic characterizations, antidiabetic, in silico and kinetic evaluation of novel curcumin-fused aldohexoses. Spectrochim Acta Part A Mol Biomol Spectrosc 285:121806
4. Kerru N, Singh-Pillay A, Awolade P, Singh P (2018) Current anti-diabetic agents and their molecular targets: A review. Eur J Med Chem 152:436–488
5. Azimi F, Ghasemi JB, Azizian H, et al (2021) Design and synthesis of novel pyrazole-phenyl semicarbazone derivatives as potential α-glucosidase inhibitor: Kinetics and molecular dynamics simulation study. Int J Biol Macromol 166:1082–1095
6. Ross SA, Gulve EA, Wang M (2004) Chemistry and biochemistry of type 2 diabetes. Chem Rev 104:1255–1282
7. Mandal AK (2015) In treating diabetes, what is important? Glucose levels or outcome measures? World J Diabetes 6:1243–1245. https://doi.org/10.4239/wjd.v6.i13.1243
8. Xie H-X, Zhang J, Li Y, et al (2021) Novel tetrahydrobenzo [b] thiophen-2-yl) urea derivatives as novel α-glucosidase inhibitors: Synthesis, kinetics study, molecular docking, and in vivo anti-hyperglycemic evaluation. Bioorg Chem 115:105236
9. Standl E, Schnell O (2012) Alpha-glucosidase inhibitors 2012–cardiovascular considerations and trial evaluation. Diabetes Vasc Dis Res 9:163–169

10. Elferink H, Bruekers JPJ, Veeneman GH, Boltje TJ (2020) A comprehensive overview of substrate specificity of glycoside hydrolases and transporters in the small intestine: “A gut feeling.” Cell Mol Life Sci 77:4799–4826

11. Shahzad D, Saeed A, Larik FA, et al (2019) Novel C-2 symmetric molecules as α-glucosidase and α-amylase inhibitors: design, synthesis, kinetic evaluation, molecular docking and pharmacokinetics. Molecules 24:1511

12. Liu Z, Ma S (2017) Recent Advances in Synthetic α-Glucosidase Inhibitors. ChemMedChem 12:819–829

13. Hosseini Nasab N, Azimian F, Kruger HG, Kim SJ (2022) Coumarin-Chalcones Generated from 3-Acetylcoumarin as a Promising Agent: Synthesis and Pharmacological Properties. ChemistrySelect 7:e202200238

14. Mahapatra DK, Bharti SK, Asati V (2017) Chalcone derivatives: anti-inflammatory potential and molecular targets perspectives. Curr Top Med Chem 17:3146–3169

15. Modzelewska A, Pettit C, Achanta G, et al (2006) Anticancer activities of novel chalcone and bis-chalcone derivatives. Bioorg Med Chem 14:3491–3495

16. K Sahu N, S Balbhadra S, Choudhary J, V Kohli D (2012) Exploring pharmacological significance of chalcone scaffold: a review. Curr Med Chem 19:209–225

17. Kumar H, Devaraji V, Joshi R, et al (2015) Antihypertensive activity of a quinoline appended chalcone derivative and its site specific binding interaction with a relevant target carrier protein. RSC Adv 5:65496–65513

18. Fu Y, Liu D, Zeng H, et al (2020) New chalcone derivatives: synthesis, antiviral activity and mechanism of action. RSC Adv 10:24483–24490

19. Choudhary AN, Juyal V (2011) Synthesis of chalcone and their derivatives as antimicrobial agents. Int J Pharm Pharm Sci 3:125–128

20. Chinthala Y, Thakur S, Tirunagari S, et al (2015) Synthesis, docking and ADMET studies of novel chalcone triazoles for anti-cancer and anti-diabetic activity. Eur J Med Chem 93:564–573

21. Mahapatra DK, Asati V, Bharti SK (2015) Chalcones and their therapeutic targets for the management of diabetes: structural and pharmacological perspectives. Eur J Med Chem 92:839–865

22. Seo WD, Kim JH, Kang JE, et al (2005) Sulfonamide chalcone as a new class of α-glucosidase inhibitors. Bioorg Med Chem Lett 15:5514–5516

23. Cai C-Y, Rao L, Rao Y, et al (2017) Analogues of xanthones——Chalcones and bis-chalcones as α-glucosidase inhibitors and anti-diabetes candidates. Eur J Med Chem 130:51–59

24. Dua R, Shrivastava S, Sonwane SK, Srivastava SK (2011) Pharmacological significance of synthetic heterocycles scaffold: a review. Adv Biol Res (Rennes) 5:120–144

25. Guo X-Y, Liu G (2013) Scaffold-hopping strategy toward calanolides with nitrogen-containing heterocycles. Chinese Chem Lett 24:295–298

26. Su J, Tang H, McKittrick BA, et al (2006) Modification of the Clozapine structure by Parallel Synthesis. Bioorg Med Chem Lett 16:4548–4553

27. Mercolini L, Protti M, Fulgenzi G, et al (2014) A fast and feasible microextraction by packed sorbent (MEPS) procedure for HPLC analysis of the atypical antipsychotic ziprasidone in human plasma. J Pharm Biomed Anal 88:467–471

28. Lin J-C, Ho Y-S, Lee J-J, et al (2007) Induction of apoptosis and cell-cycle arrest in human colon cancer cells by meclizine. Food Chem Toxicol 45:935–944

29. Abdelrahman MM (2013) Simultaneous determination of Cinnarizine and Domperidone by area under curve and dual wavelength spectrophotometric methods. Spectrochim Acta Part A Mol Biomol Spectrosc 113:291–296

30. Kálai T, Khan M, Balog M, et al (2006) Structure–activity studies on the protection of Trimetazidine derivatives modified with nitroxides and their precursors from myocardial ischemia–reperfusion injury. Bioorg Med Chem 14:5510–5516

31. Malati V, Reddy AR, Mukkanti K, Suryanarayana M V (2012) A novel reverse phase stability indicating RP-UPLC method for the quantitative determination of fifteen related substances in Ranolazine drug substance and drug product. Talanta 97:563–573

32. Sui W, Yang X, Yu W, et al (2014) A validated LC–MS/MS method for the rapid quantification of vilazodone in rat plasma: Application to a pharmacokinetic study. J Pharm Biomed Anal 98:228–234

33. Yonar D, Sünnetçioğlu MM (2014) Spectroscopic and calorimetric studies on trazodone hydrochloride–phosphatidylcholine liposome interactions in the presence and absence of cholesterol. Biochim Biophys Acta (BBA)-Biomembranes 1838:2369–2379

34. Manley PW, Blasco F, Mestan J, Aichholz R (2013) The kinetic deuterium isotope effect as applied to metabolic deactivation of imatinib to the des-methyl metabolite, CGP74588. Bioorg Med Chem 21:3231–3239

35. Ananda Kumar CS, Nanjunda Swamy S, Thimmegowda NR, et al (2007) Synthesis and evaluation of 1-benzhydryl-sulfonyl-piperazine derivatives as inhibitors of MDA-MB-231 human breast cancer cell proliferation. Med Chem Res 16:179–187

36. Tagat JR, McCombie SW, Steensma RW, et al (2001) Piperazine-based CCR5 antagonists as HIV-1 inhibitors. I: 2 (S)-methyl piperazine as a key pharmacophore element. Bioorg Med Chem Lett 11:2143–2146

37. Wang T, Kadow JF, Zhang Z, et al (2009) Inhibitors of HIV-1 attachment. Part 4: A study of the effect of piperazine substitution patterns on antiviral potency in the context of indole-based derivatives. Bioorg Med Chem Lett 19:5140–5145

38. Kulig K, Sapa J, Nowaczyk A, et al (2009) Design, synthesis and pharmacological evaluation of new 1-[3-(4-arylpiperazin-1-yl)-2-hydroxy-propyl]-3, 3-diphenylpyrrolidin-2-one derivatives with antiarrhythmic, antihypertensive, and α-adrenolytic activity. Eur J Med Chem 44:3994–4003

39. Oh K-S, Oh BK, Park CH, et al (2013) Cardiovascular effects of a novel selective Rho kinase inhibitor, 2-(1H-indazole-5-yl) amino-4-methoxy-6-piperazino triazine (DW1865). Eur J Pharmacol 702:218–226

40. Sharma SK, Panneerselvam A, Singh KP, et al (2016) Teneligliptin in management of type 2 diabetes mellitus. Diabetes, Metab Syndr Obes targets Ther 9:251–260

41. Nasab NH, Azimian F, Eom YS, et al (2023) Synthesis, anticancer evaluation, and molecular docking studies of thiazolyl-pyrazoline derivatives. Bioorg Med Chem Lett 80:129105

42. Nasab NH, Raza H, Eom YS, et al (2023) Design, synthesis, and in vitro and in silico studies of 1, 3, 4-thiadiazole-thiazolidinone hybrids as carbonic anhydrase inhibitors. New J Chem 47:13710–13720

43. Nasab NH, Raza H, Eom YS, et al (2023) Design and synthesis of thiadiazole-oxadiazole-acetamide derivatives: Elastase inhibition, cytotoxicity, kinetic mechanism, and computational studies. Bioorg Med Chem 86:117292

44. Nasab NH, Raza H, Eom YS, et al (2023) Synthesis and discovery of potential tyrosinase inhibitor of new coumarin-based thiophenyl-pyrazolylthiazole nuclei: in-vitro evaluation, cytotoxicity, kinetic and computational studies. Chem Biol Drug Des 101:1262–1272

45. Hosseini Nasab N, Raza H, Shim RS, et al (2022) Potent Alkaline Phosphatase Inhibitors, Pyrazolo-Oxothiazolidines: Synthesis, Biological Evaluation, Molecular Docking, and Kinetic Studies. Int J Mol Sci 23:13262. https://doi.org/10.3390/ijms232113262

46. Nasab NH, Raza H, Hassan M, et al (2023) A facile green synthesis of 3, 4-dihydropyrimidin-2 (1H)-ones using cysteine as a bio-organic catalyst: Potent urease inhibitors, in vitro evaluation, kinetic mechanism, and molecular docking studies. J Mol Struct 1286:135638

47. Li J, Li D, Xu Y, et al (2017) Design, synthesis, biological evaluation, and molecular docking of chalcone derivatives as anti-inflammatory agents. Bioorg Med Chem Lett 27:602–606

48. Li Y, Tang Y, Li M, et al (2020) Synthesis and antibacterial activity of thienyl chalcone derivatives bearing piperazine moiety. Chinese J Org Chem 40:108–114

49. Hosseini Nasab N, Azimian F, Eom YS, et al (2023) Synthesis, anticancer evaluation, and molecular docking studies of thiazolyl-pyrazoline derivatives. Bioorg Med Chem Lett 80:129105

50. Hosseini Nasab N, Raza H, Eom YS, et al (2023) Synthesis and discovery of potential tyrosinase inhibitor of new coumarin-based thiophenyl-pyrazolylthiazole nuclei: in-vitro evaluation, cytotoxicity, kinetic and computational studies. Chem Biol Drug Des 101:1262–1272. https://doi.org/10.1111/cbdd.14209

51. Abbas Q, Hassan M, Raza H, et al (2017) In vitro, in vivo and in silico anti-hyperglycemic inhibition by sinigrin. Asian Pac J Trop Med 10:372–379

52. Hosseini Nasab N, Raza H, Shim RS, et al (2023) A facile green synthesis of 3, 4-dihydropyrimidin-2 (1H)-ones using cysteine as a bio-organic catalyst: Potent urease inhibitors, in vitro evaluation, kinetic mechanism, and molecular docking studies. J Mol Struct 1286:135638

53. Jejurikar BL, Rohane SH (2021) Drug designing in discovery studio. indianjournals.com 14:135–138. https://doi.org/10.5958/0974-4150.2021.00025.0

54. O'Boyle NM, Banck M, James CA, et al (2011) Open Babel: An open chemical toolbox. J Cheminform 3:1–14

55. Schüttelkopf AW, Van Aalten DMF (2004) PRODRG: a tool for high-throughput crystallography of protein–ligand complexes. Acta Crystallogr Sect D Biol Crystallogr 60:1355–1363

56. Xu D, Zhang Y (2011) Improving the physical realism and structural accuracy of protein models by a two-step atomic-level energy minimization. Biophys J 101:2525–2534

57. Hsu K-C, Chen Y-F, Lin S-R, Yang J-M (2011) iGEMDOCK: a graphical environment of enhancing GEMDOCK using pharmacological interactions and post-screening analysis. BMC Bioinformatics 12:S:33. https://doi.org/10.1186/1471-2105-12-S1-S33

58. Pires DE V, Blundell TL, Ascher DB (2015) pkCSM: predicting small-molecule pharmacokinetic and toxicity properties using graph-based signatures. J Med Chem 58:4066–4072

59. Daina A, Michielin O, Zoete V (2017) SwissADME: a free web tool to evaluate pharmacokinetics, drug-likeness and medicinal chemistry friendliness of small molecules. Sci Rep 7:42717

Supplementary Files

This is a list of supplementary files associated with this preprint. Click to download.

- SupportingInformation.docx